Journal of Energy Chemistry 25 (2016) 798–804

Contents lists available at ScienceDirect

Journal of Energy Chemistry

journal homepage: www.elsevier.com/locate/jechem

http://www.journals.elsevier.com/journal-of-energy-chemistry/

Photoelectrochemical study of MoO_3 assorted morphology films formed by thermal evaporation

R. Senthilkumar[a], G. Anandhababu[a], T. Mahalingam[b], G. Ravi[a,*]

[a] Department of Physics, Alagappa University, Karaikudi 630004, India
[b] Department of Electrical and Computer Engineering, Ajou University, Suwon 443-749, South Korea

ARTICLE INFO

Article history:
Received 25 December 2015
Revised 3 February 2016
Accepted 8 February 2016
Available online 26 April 2016

Keywords:
Molybdenum oxide
Thermal evaporation
Nanostructure
Photoelectrochemical cell

ABSTRACT

Molybdenum oxide nanostructured thin films were grown on fluorine doped tin oxide (FTO), indium doped tin oxide (ITO) and ordinary glass substrates by thermal evaporation process without vacuum and catalysts using molybdenum trioxide (MoO_3) powder as a source material and oxygen as a carrier gas. Various morphologies including nanobelts, disks and hexagonal rod-like nanostructures were obtained by changing the source and substrate temperatures during the growth of MoO_3 thin films. Structural parameters, morphology, composition and surface features of the films were characterized by XRD, SEM, EDAX, XPS, AFM and Raman spectroscopy. The films were orthorhombic in structure with preferred orientation along (0 1 0) plane. Morphology analysis reveals randomly aligned nanobelts with 40 nm in thickness and a width of 800 nm and 3–12 mm in length. The disks have 1.5 μm diameters, 1 μm thickness and hexagonal rod-like nanostructures with a length, breath and width of 2 μm, 1 μm and 100 nm are formed. The samples were investigated under dark and photocurrent conditions in H_2SO_4 aqueous solution as a function of applied potential. The photocurrent density of samples prepared on ITO and FTO substrate samples were compared and the results are discussed.

1. Introduction

Solar energy is able to meet global demand of power by several orders of magnitude. Hence, a current priority in solar energy research is to generate energy in the form of electricity [1–6]. Particularly, Photo Electrochemical Cell (PEC) is most efficient method of harvesting solar power. Most metal oxides such as MoO_3, WO_3, V_2O_5, TiO_2 and SnO_2 play vital role in solar energy conversion process. These metal oxides generate a pair of electron and hole per absorbed photon when the energy of the incident photon is higher than the band gap of the material. This property has been successfully used to convert solar energy into electrical energy by photovoltaic devices [7–10].

Molybdenum oxide (MoO_3) is one of the very important types of semiconducting materials which possess excellent electrochromic, optochromic, and gasochromic properties [11–15]. In the past, MoO_3 has been used to manufacture various devices such as flat-panel displays, electrochromic smart windows, optical modulation devices, write–read–erase optical devices, sensors and field emission devices [16–21]. To date, molybdenum oxide is the benchmark semiconductor for PEC application due to its chemical stability and high activity. Crystal size, surface area and morphology are the important aspects in the development of such device applications.

A number of techniques were reported for the deposition of MoO_3, including pulsed laser deposition, thermal evaporation (vapor–soild and vapor–liquid–solid), sputtering, spray pyrolysis, chemical vapor deposition, hydrothermal and electrode position. Among these techniques, the deposition of MoO_3 using vapor solid process offers greater advantages as they could produce highly crystalline and nano dimensional structures. Vapor–solid growth is historically based on the formation of whiskers. Whisker growth is a crystalline phenomenon whereby tiny metal grows and filiform hairs are formed on the surface of substrate. The vapor–solid mechanism is a catalyst free process whereas the sublimated vapor created by heating the source powder is transported to lower temperature zone and get deposited on the substrate to form nanostructure [22,23].

In this work, we report the synthesis of molybdenum oxide nanostructures such as nanobelts, nanodisks and hexagonal rod-like by vapor–solid process on FTO, ITO and glass substrates at ambient pressure in a flow of O_2. The structural property of synthesized MoO_3 thin films was characterized by X-ray diffraction (XRD) analysis using a PANalytical model X'PERT-PRO X-ray diffrac-

* Corresponding author. Tel: +91 4565 230251; Fax: +91 4565 225202.
E-mail addresses: raviganesa@rediffmail.com, gravicrc@gmail.com (G. Ravi).

http://dx.doi.org/10.1016/j.jechem.2016.04.005

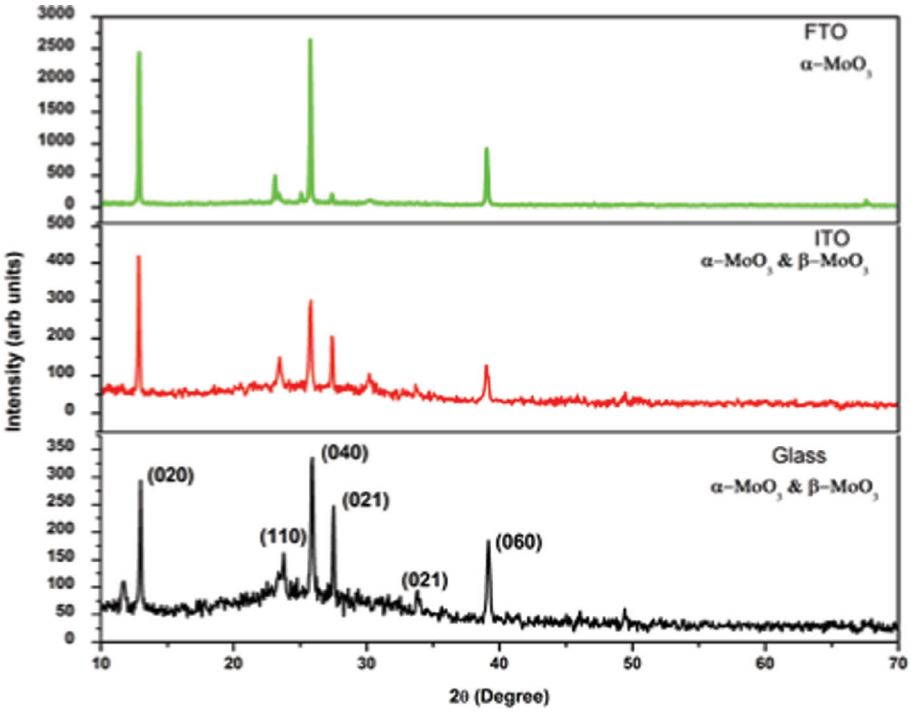

Fig. 1. XRD patterns of MoO_3 film deposited on glass, ITO and FTO substrates.

tometer system with the *Kα* radiations from a copper target (λ = 1.5418 Å). The surface morphology of the thin films was examined using scanning electron microscope (SEM) (JSM 6390F, JEOL/EO) and transmission electron microscope (TEM) (JSM 6390F, JEOL/EO). The film composition was confirmed by energy dispersive X-ray spectroscopy (EDAX). Raman spectrum was recorded using an imaging spectrograph STR 500 mm focal length laser Raman spectrometer (SEKI, Japan). X-ray photoelectron spectrometry (XPS) analysis was used to analyze the presence of metal-oxygen (SEKI, Japan). Photocurrent density, incident photon-to-current efficiency (IPCE) and photoconversion efficiency were measured by an electrochemical analyzer (Autolab PGSTAT30, Tennison Hill Drive Austin, USA) in a standard three electrode configuration with a platinum foil as counter electrode, a saturated calomel electrode (SCE) as reference electrode, and MoO_3 thin film as photoanode. The potential was swept linearly at a scan rate of 20 mV/s. A 1 kW mercury lamp (Austin, USA) served as the UV light source, with an AM1 filter to simulate solar conditions. Linear sweep voltammograms were measured in the potential range of −1.0 V to +1.6 V at a scan rate of 10 mV/s.

2. Experimental

Molybdenum oxide nanostructured thin films were grown by a thermal evaporation method. Molybdenum tri-oxide powder (MoO_3) was used as the source material. A quartz tube is fixed in a horizontal tubular furnace (Thermolyne-4700) without vacuum system. 2 g Molybdenum tri oxide powder was sprinkled in an alumina boat and placed at a constant high temperature maintained area of the quartz tube. Indium tin oxide coated glass (ITO), fluorine doped tin oxide coated glass (FTO) and ordinary glass substrates were positioned at 22–27 cm distance from the alumina boat along one side of the quartz tube. The temperature of the tubular furnace was increased at a constant rate of 10 °C/min from room temperature to source vaporizing temperature at 720 °C. After attaining the vaporizing temperature, an oxygen flow of 50 sccm was admitted through the quartz tube, introduced by the side closer to the molybdenum oxide source and maintained for 6 h. In the mean time, the substrate temperature was maintained around 450 °C. Next, the temperature of the tubular furnace was constantly decreased at a constant rate of 30 °C/min from the source vaporization temperature to room temperature. During the process, molybdenum oxide powder was heated and vaporized in the higher temperature zone and deposited onto the substrates at the lower temperature zone [24,25].

3. Results and discussion

3.1. Structural analysis

The X-ray diffraction patterns of molybdenum oxide thin films deposited on different substrates at 450 °C are shown in Fig. 1. These patterns exhibit several peaks along different orientation planes including three dominant planes (020), (040) and (060). This reveals that the samples are polycrystalline in nature. The film deposited on FTO substrate exhibits α-MoO_3 orthorhombic structure as confirmed from JCPDS index (Card no: 05-508) with cell parameters, a = 3.962 Å, b = 13.850 Å, c = 3.697 Å. The strong diffraction peaks appear at 2θ angles 12.9°, 25.8° and 39.1° correspond to the (020), (040) and (060) planes, respectively. Films on glass and ITO substrates exhibit (110) and (021) peaks with less intensity and indexed to β-MoO_3 crystal structure using JCPDS data (Card No. 65-2421). The film on FTO substrate exhibits higher intensity and consist of only orthorhombic α-MoO_3 structure [26–28].

The crystallite size (D), dislocation density (δ) and strain (ε) are calculated using the relations:

$$D_{hkl} = \frac{k\lambda}{\beta \cos\theta} \quad (1)$$

$$\delta = \frac{1}{D^2} \quad (2)$$

$$\varepsilon = \frac{\beta \cos\theta}{4} \quad (3)$$

A comparison of average particle size, microstrain and dislocation density of the thin films coated on glass, ITO and FTO sub-

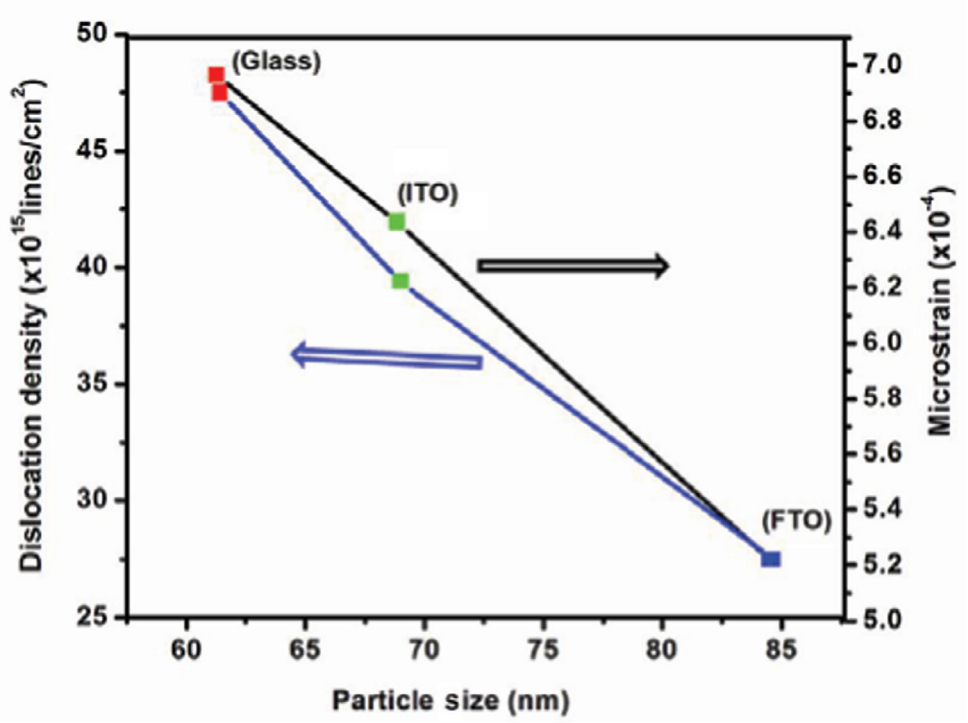

Fig. 2. Comparison of particle size, microstrain and dislocation density of MoO_3 film deposited on glass, ITO and FTO substrates.

strates are shown in Fig. 2. It is observed that the average particle size is maximum around 84.6 nm for film coated on FTO substrate and 68.4 and 62.3 nm for films coated on ITO and glass substrates. At the same time, the microstrain and dislocation density are minimum for thin film coated on FTO substrate and maximum for thin film deposited on ITO and glass substrates.

3.2. Laser Raman spectroscopy analysis

The Raman spectra of MoO_3 thin films deposited on FTO, ITO and glass substrates at 450 °C are shown in Fig. 3. Strong Raman peaks are present at 304, 670, 822, and 993 cm^{-1} for all the samples. The peak at 304 cm^{-1} represents the bending mode for the double bond (Mo = O) vibration. The 670 cm^{-1} peak is assigned to the triply coordinated oxygen (Mo_3–O) stretching mode, which results from edge-shared oxygen atoms in common to three adjacent octahedra. The peak at 822 cm^{-1} is for the doubly coordinated oxygen (Mo_2–O) stretching mode, which results from corner-sharing oxygen atoms common to two octahedral. The peak at 993 cm^{-1} is assigned to the terminal oxygen (Mo^{6+} = O) stretching mode, which results from an unshared oxygen. Other peaks at 388 and 349 cm^{-1} can be assigned to Mo_3–O and Mo=O bending modes, while the peak at 479 cm^{-1} has the same band assignment as that of 670 cm^{-1}.

In addition, two weak peaks at 177 and 257 cm^{-1} represent the bending mode of Mo_2–O. All the thin films exhibit same wave numbers (304, 670, 822 and 993 cm^{-1}) with different intensities [29–32]. The peak positions are in good agreement with those reported in literature for the orthorhombic MoO_3 crystalline phase. The observed wavenumbers are summarized in Table 1 and compared to the reference data reported by Jian Zhen Ou et al. [33].

Table 1. Comparison of observed and reported MoO_3 Raman bands.

S.No	Observed wave numbers (cm^{-1})	Work by Jian Zhen Ou et al. (cm^{-1})	Raman groups and assignment
1	177	173	Bending mode of Mo_2–O
2	257	284	Bending mode of Mo_2–O
3	304	298	Mo_3–O and Mo = O bending modes
4	349	339	Mo_3–O and Mo = O bending modes
5	388	376	Mo_3–O and Mo = O bending modes
6	479	471	Mo_3–O stretching mode
7	670	666	Mo_3–O stretching mode
8	822	821	Mo_2–O stretching mode
9	993	995	Mo^{6+} = O stretching mode

3.3. X-ray photoelectron spectroscopy (XPS) analysis

The chemical composition of MoO_3 thin films was investigated by X-ray photoelectron spectroscopy. Fig. 6 shows the wide scan XPS spectrum with the binding energy range of 0–800 eV for MoO_3 thin films deposited on ITO and FTO substrates. The spectrum shows that the main constituent elements of annealed thin films are molybdenum and oxygen atoms. The photo-electron peaks of the main elements, Mo and O peaks were obtained, to reveal the compositional purity and quality of the MoO_3 films. The core level spectra of Mo 3*d* and O 1 *s* in MoO_3 films are analyzed. The two components associated with Mo $3d_{5/2}$ and Mo $3d_{3/2}$ *sp* in orbit doublet at 233 and 235 eV, respectively, are in agreement with previous literature reports for Mo^{6+} in MoO_3 stoichiometric thin films. The integrated areas of the Mo-3*d* and O-1 *s* peaks were used to determine the concentrations of Mo and O on the film surface. The peaks located at 416 and 398 eV were the molybdenum Mo $3P_{1/2}$ and Mo $3P_{3/2}$, respectively. The peak situated at 283 eV related to the carbon C 1 *s* due to the contamination of carbon on the surface since the films were exposed to the atmosphere. The

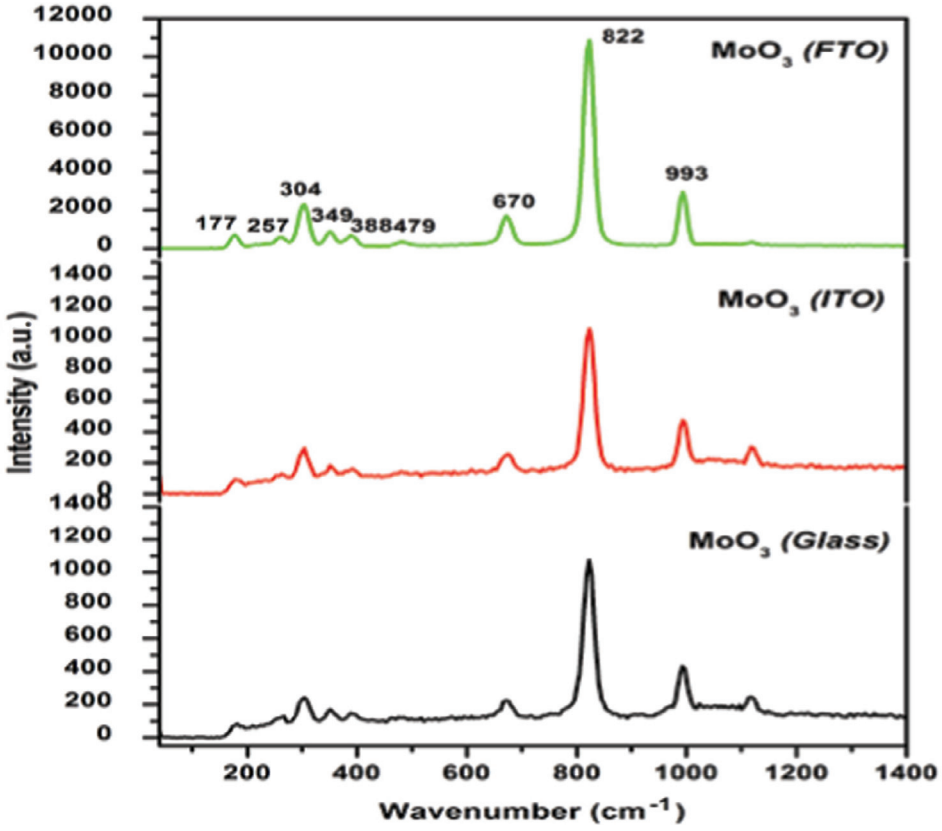

Fig. 3. Laser Raman spectra of MoO_3 thin films deposited on glass, ITO and FTO substrates.

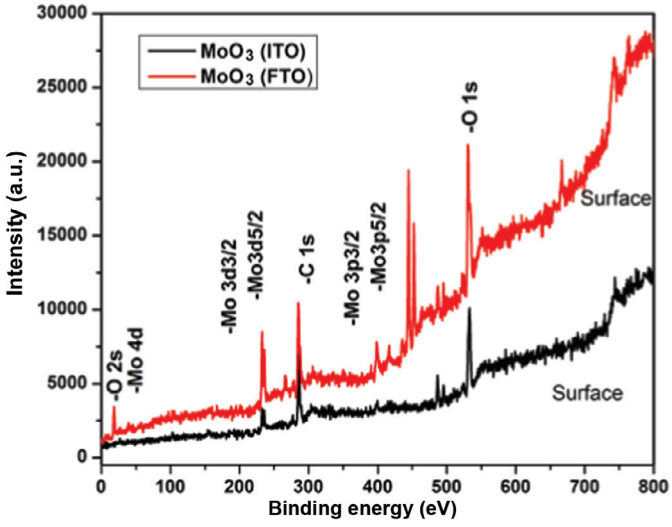

Fig. 4. XPS spectra of MoO_3 thin films deposited on ITO and FTO substrates.

peaks located at about 18 and 35 eV related to the O 2 *s* and Mo 4*d*, respectively (Fig. 4).

3.4. Scanning electron microscope analysis

Scanning electron microscope images of molybdenum oxide nanostructures such as rectangular prism, disk and belt are shown in Fig. 6. The length and breadth of these structures are several microns and the thickness is consistently in nanometer range. The formation of these nanostructures may be explained by Vapor–Solid (VS) mechanism. In our deposition method, molybdenum

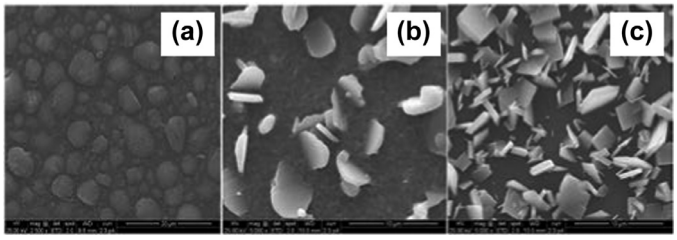

Fig. 5. SEM images of MoO_3 thin films synthesized on (a) glass, (b) ITO and (c) FTO substrates at 400 °C.

oxide vapor is created by heating the source powder at elevated temperature around 700 °C in a high temperature zone and transported to a lower temperature zone 400–450 °C through carrier gas (O_2). During this period vapors are adhered onto the substrates such as glass, ITO and FTO substrates to form film. The formation of different morphological nanostructures is influenced by the synthesis factors such as source and substrate temperature and carrier gas in vapor solid process. The substrate temperature plays a vital role in controlling the nucleation and growth of MoO_3 nanostructures [34–36] and it determines how much vapors condensed to form nanostructures. The substrate temperature is varied by changing the position of the substrates from the source in the tubular furnace. The nucleation process depends on the interfacial energies between the substrate and vapors reacting on it.

At substrate temperature below 400 °C fewer amount of vapor is condensed on their surface. Initially, vapors are adhered onto the substrate surface and create isolated patches. Subsequently, these isolated patches coalesces and grow together to form randomly aligned roomy leaves and morsel like structures as shown in Fig. 5(b) and (c). The ITO and FTO substrates are previously

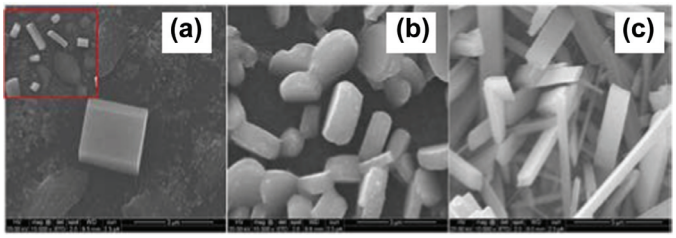

Fig. 6. SEM images of MoO_3 thin films synthesized on (a) glass, (b) ITO and (c) FTO substrates at 450 °C.

coated with few microns of indium and fluorine doped tin oxide, respectively. It interacts with more molybdenum oxide vapors and easily facilitates the growth of crystal structure. Even though MoO_3 was coated onto glass substrates, vapors do not easily interact and condense on their surface which results no specific morphology was formed as shown in Fig. 5(a). When the substrate temperature is increased in the range of 400–450 °C more vapor is condensed onto the substrates and well cleared crystalline structures such as belt, disk and hexagonal rods are formed as shown in Fig. 6. The nanobelts are highly dense with asymmetrical distribution as revealed by the magnified image of a top view shown Fig. 6(c). The nanobelts are straight and smooth, about 3–5 μm length with diameters ranging from 40 to 350 nm. The disk with an average length, breath and width of 1.5 μm, 1 μm and 500 nm, respectively is found on ITO substrate as shown in Fig. 6(b). The hexagonal rods (inset Fig. 6a) with a length, breath and width of 2 μm, 1 μm and 100 nm are formed on glass substrate as shown in Fig. 6(a). The thickness of the ITO and glass substrates were lesser (around 2 mm) compared to FTO (4.2 mm). Both substrates were heated rapidly and they adsorbed more vapor to form blurred crystal structures. FTO substrates were steadily heated and molecules were one by one to form well aligned morphology [37].

As can be seen from the SEM images, the morphology of MoO_3 thin films differs depending on the type of substrates. Such morphology difference can be explained by the difference in the surface level of the substrates. Higher density grains on the FTO substrate provoke large amount of nuclei that can further coalescence and promote the lateral growth of the crystal. The resistivity of the substrates might also play a role for the difference in final shape of the MoO_3 crystals. In our case, the ITO has lower resistivity (ρ∼15–20 Ω/cm) than FTO substrate (ρ∼150 Ω/cm) that conductive substrates greatly affect the structural properties of MoO_3 thin films.

3.5. Compositional analysis

The energy dispersive X-ray analysis (EDAX) of MoO_3 thin films prepared on FTO, ITO and glass substrates is shown in Fig. 7. It is observed that molybdenum and oxygen are present, indicating that the nanostructures are composed only by Mo and O atoms. Fig. 8 shows the molecular weight of molybdenum and oxygen content in MoO_3 thin films prepared on FTO, ITO and glass substrates. Thin film deposited on FTO substrate reveals good O/Mo weight ratio nearly equalent to 3. It is found that MoO_3 thin films synthesized on FTO substrates possess good stoichiometry compared to films prepared on ITO and glass substrates [38,39].

3.6. Atomic force microscope analysis

The surface topography studies on MoO_3 films were carried out using an atomic force microscope. AFM images of films deposited on ITO and FTO at a substrate temperature 450 °C are shown in Fig. 9. MoO_3 thin films prepared on ITO substrate with 300 nm

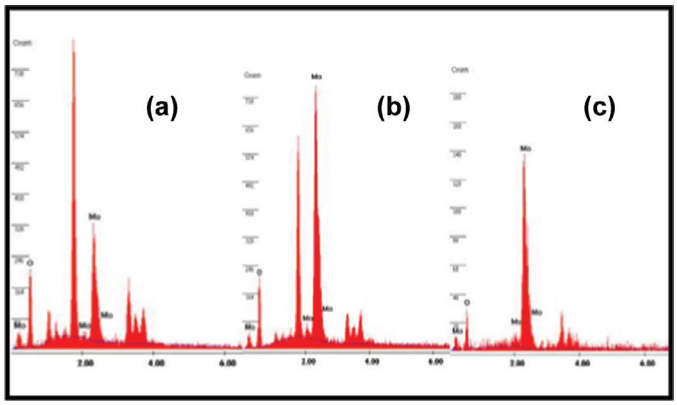

Fig. 7. EDAX spectra of MoO_3 deposited on (a) glass, (b) ITO and (c) FTO substrates.

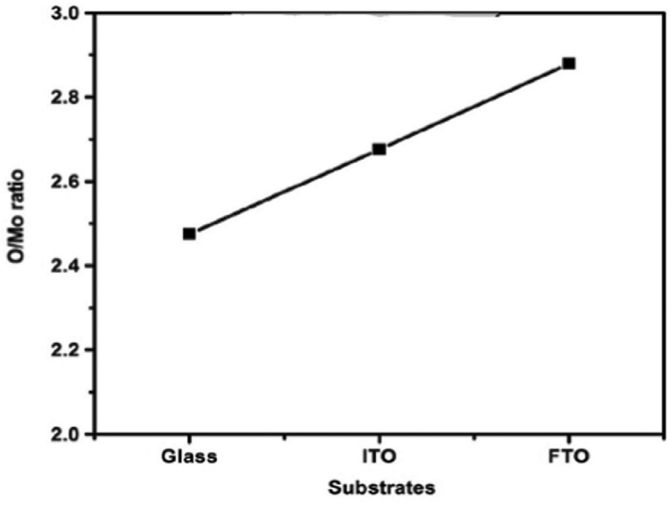

Fig. 8. Atomic percentage of MoO_3 thin films prepared on glass, ITO and FTO substrates.

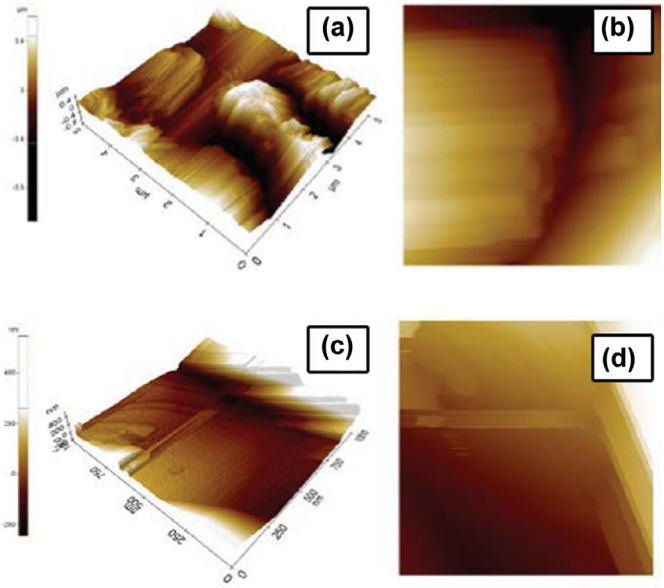

Fig. 9. AFM 2D and 3D view of MoO_3 on ITO (a) and (b), and FTO (c) and substrates (d).

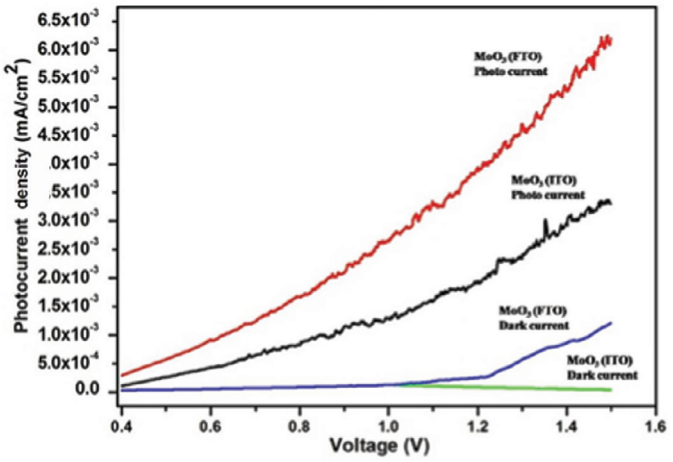

Fig. 10. *I-V* characteristics of PEC solar cells of MoO_3 thin films on ITO and FTO substrates.

thickness exhibit combined plates like hillock structures of the order of 1–2 μm length and breadth as shown in Fig. 9(a). During the initial stage of synthesis, the molecules are attached to form column like nanorods and the rods collaged together to form bulk plates or hillock structures as shown in two dimensional topography view in Fig. 9(b).

At the same time, relatively flat uniform surface in the form of rectangular nanobelts is formed on FTO substrate as shown in Fig. 9(c). No agglomerated grains are viewed on the surface of nanobelts and it is highly smooth as shown in Fig. 9(d). FTO substrate was fully covered with nanobelts directed towards various directions (more MoO_3 molecules are attached) and the roughness is higher in the order of 0.79 Å compared to ITO substrate (0.54 Å) [40–42].

3.7. Photoelectrochemical study

The photoelectrochemical (PEC) measurements were carried out in a potentiostatic system (Autolab PGSTAT30) with molybdenum oxide film as the working electrode, platinum as the counter electrode and a saturated calomel electrode (SCE) as a reference electrode. All potentials are measured against SCE. An aqueous solution of 0.5 M H_2SO_4 was used as the electrolyte and irradiation was provided by a 1 kW Xe arc lamp with an AM1 filter to simulate solar conditions. For monochromatic irradiation experiments, a monochromator was positioned between the source and the photoelectrochemical cell. Linear sweep voltammograms were measured, scanning from −1.0 V to +1.6 V at a scan rate 10 mV/s [43–48].

Photoconductivity is a phenomenon in which samples become electrically conductive to the illumination of light. When light is absorbed by the sample, the number of free electrons and holes changes and raises its electrical conductivity. Photo current density response results under dark and illumination condition are shown in Fig. 10. It is observed that photo current of all the samples increases dramatically with applied bias voltage. The light is illuminated on the samples under a positive potential and electrons are continuously released with increase in photo current. The photocurrent of MoO_3 thin film on FTO substrate is found to be 6.2 mA/cm^2. This is 2 times greater than for the MoO_3 thin film coated on ITO. Under the dark condition no measurable current was detected for both the MoO_3 thin films up to the bias voltage 1.25 V. When the applied voltage is increased, MoO_3 thin film on FTO substrate conducts weak current around 1 mA/cm^2. The dark current of MoO_3 thin film on ITO substrate remains unchanged.

Table 2. Power output characteristics of MoO_3 thin film based photoelectrochemical solar cell.

Sl. No.	MoO_3 thin films substrate	I_{sc} (A/cm^2)	I_{MP} (m^{-2})	V_{OC} (V)	V_{MP} (V)	FF (%)
1	ITO	3.3×10^{-6}	1.6×10^{-3}	1.25	1.20	0.48
2	FTO	6.3×10^{-3}	4.6×10^{-3}	1.25	1.20	0.70

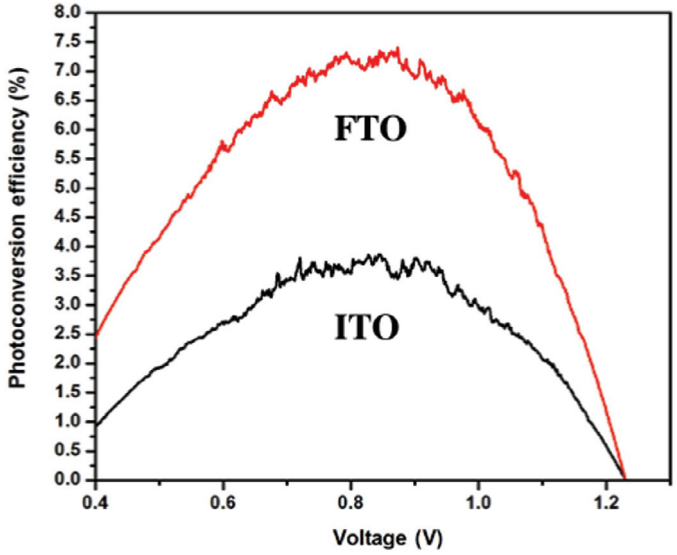

Fig. 11. Photoconversion efficiency of MoO_3 thin films on ITO and FTO substrates.

Samples are found to be responsive only under the illumination of light. It indicates that MoO_3 films are photoconductive in nature. The photosensitivity of samples was determined using the relation $S = \sigma h/\sigma d$ and calculated to be 4.79 and 3.64 for FTO and ITO sample, respectively. The measurement of incident photon-to-current-conversion efficiency (IPCE) is defined as a percentage quantity of the number of collected excited electrons over the number of incident monochromatic photons. The incident photon-to-current efficiency (IPCE) was calculated from the following equation [49–51].

$$\mathrm{IPCE}(\%) = \frac{1240 J_{ph} \times 100}{\lambda P_0} \tag{4}$$

where J_{ph} is the photo current density (mA/cm^2), 'λ' is the wavelength of the incident light (nm) and P_0 is the incident light power density (mW/cm^2). The fill factor (FF) is essentially a measure of the PEC cell quality. The FF values are calculated by the following equation and tabulated in Table 2.

$$\mathrm{FF} = \frac{V_{MP} \cdot I_{MP}}{V_{OC} \cdot I_{SC}} \tag{5}$$

where V_{OC} is the open circuit potential (V), I_{SC} is the short-circuit current density (A/cm^2), I_{MP} is the maximum current at the maximum power output point (A/cm^2) and V_{MP} is the maximum voltage at the maximum power output point (V).

The photoconversion (light energy to electrical energy) efficiency ($\varepsilon_{\mathrm{eff}}$) of PEC in the presence of a bias potential was calculated from the following equation as shown in Fig. 11.

$$\varepsilon_{\mathrm{eff}}(\mathrm{photo})(\%) = J_p[E^o_{\mathrm{rev}} - |E_{\mathrm{app}}|] \times 100/(I_o) \tag{6}$$

where J_p is the photocurrent density (mA/cm^2), $E_{\mathrm{rev}}{}^0$ is the standard reversible potential (1.23 V), I_0 is the power density of the incident light (mW/cm^2) and $|E_{\mathrm{app}}|$ is the absolute value of the applied potential E_{app}, which is obtained from the following equation

$$E_{\mathrm{app}} = (E_{\mathrm{meas}} - E_{\mathrm{ocp}}) \tag{7}$$

where E_{meas} is the electrode potential of the working electrode at which J_p was measured under illumination and E_{ocp} is the applied potential at open circuit under the same illumination at which J_p was measured [52–54]. The photoconversion efficiency of FTO substrate substrate MoO_3 film was 7.3%. This efficiency was 2.1 times larger than the value obtained for the film on ITO substrate (3.4 %).

MoO_3 thin films deposited on FTO and ITO substrates exhibit different nanostructures such as nanobelt and nanodisk respectively. MoO_3 thin films on FTO substrate have higher surface to volume ratio. The surface to volume ratio plays a significant effect on the photocurrent measurement. Further, the enrichment of photocurrent and photoconversion efficiency was observed for MoO_3 thin film on FTO substrate because more molecules were accumulating on their surface. The nanobelts occupied with well defined morphology with porous nature are suitable to achieve higher photoconversion efficiency. This result shows that the thin films deposited on FTO substrates generates more photo current than the thin films deposited on ITO substrates which makes them promising candidates for solar cells.

4. Conclusions

In this work, we report an inexpensive method to produce nanocrystalline molybdenum oxide thin film with different morphology including belt, diskette and rectangular prism on FTO, ITO and glass substrates. The substrates temperature plays a vital role to the formation of different nanostructures. XRD results showed that films are polycrystalline with α-orthorhombic structure. The chemical composition and stoichiometry of the film was confirmed. Surface analysis indicates that film coated on FTO substrate was fully covered with randomly aligned nanobelt and mean roughness was higher compared to films on ITO and glass substrates. MoO_3 thin film on FTO substrate exhibited higher photocurrent (6.2 mA/cm^2) and photoconversion efficiency (7.3%) under the illumination of light compared with film on ITO substrate (3.35 mA/cm^2 and 3.4%). Our results indicate that MoO_3 film synthesized on FTO exhibits promising properties for photochromic device applications.

References

[1] E. Comini, G. Faglia, G. Sberveglieri, Z. Pan, Z.L. Wang, Appl. Phys. Lett. 81 (2002) 1869–1871.
[2] P. Ivanov, J. Hubalek, K. Malysz, J. Prasek, X. Vilanova, E. Llobet, X Correig, Sens. Actuators B. 100 (2004) 221–227.
[3] Ghenadii Korotcenkov, Mater. Sci. Eng. B. 139 (2007) 1–23.
[4] S.M. Kanan, C.P. Tripp, Langmuir 18 (2002) 722–728.
[5] Neha Desai, Sawanta Mali, Vijay Kondalkar, Rahul Mane, Chang Hong, Popatrao Bhosale, J. Nanomed. Nanotechnol 6 (2015) 1–7.
[6] Popatrao N. Bhosale, et al., RSC Adv 5 (2015) 40283–40296.
[7] Kai Huang, Qingtao Pan, Feng Yang, Shibi Ni, Deyan He, Appl. Surf. Sci. 253 (2007) 8923–8927.
[8] Yong Shin Kim, Sens. Actuators B 137 (2009) 297–304.
[9] Camelia Matei Ghimbeu, Martine Lumbreras, Maryam Siadat, Joop Schoonman, Mater. Sci. Semi. Proc. 13 (2010) 1.
[10] Wei-De Zhang, Wen-Hui Zhang, Xue-Yong Ma, J. Mater. Sci 44 (2009) 4677–4682.
[11] Shih Yuan Lin, Ying Chung Chen, Chih Ming Wang, Po-Tsung Hsieh, Shun–Chou Shih, Appl. Surf. Sci. 255 (2009) 3868–3874.
[12] E. Comini, G. Sberveglieri, M. Ferroni, V. Guidi, G. Martinelli, Sens. Actuators B. 93 (2003) 409–414.
[13] V. Nirupama, M. Chandrasekhar, P. Radhika, B. Sreedhar, S. Uthanna, J. Optoelectron. Adv. Mater. 11 (2009) 320–325.
[14] R.S. Patil, M.D. Uplane, P.S. Patil, Int. J. Electrochem. Sci. 3 (2008) 259–265.
[15] Hoa Nguyen, A. Sherif, El-Safty, J. Phys. Chem. C. 115 (2011) 8466–8474.
[16] Mehdi Ranjbar, Azamlraji zad, Seyyed Mohammad, Mahdavi, Appl. Phys. A. 92 (2008) 627–634.
[17] P.A. Spevack, N.S. Mcintyre, J. Phys. Chem. 96 (1992) 9029–9035.
[18] Kishorkumar V. Khot, Sawanta S. Mali, Rohini R. Kharade, Rahul M. Mane, Pramod S. Patil, Chang Kook Hong, Jin Hyeok Kim, Jaeyeong Heo, Popatrao N. Bhosale, J. Mater. Sci.: Mater. Electron 25 (2014) 5606–5617.
[19] K.V. Khot, S.S. Mali, R.M. Mane, P.S. Patil, Chang Kook Hong, Jin Hyeok Kim, Jaeyeong Heo, Popatrao N. Bhosale, J. Mater. Sci.: Mater. Electron 26 (2015) 6897–6906.
[20] Yung-Sen Lin, Jhen-Yi Lai, Tsung-Hsien Tsai, Pei-Ying Chuang, Yen- Cheng Chen, Thin Solid Films 519 (2011) 3875–3882.
[21] Sobia Ashraf, Christopher S. Blackman, Geoffrey Hyett, Ivan P. Parkin, J. Mater. Chem. 16 (2006) 3575–3582.
[22] T. Siciliano, A. Tepore, E. Filippo, G. Micocci, M. Tepore, Mater. Chem. Phys. 114 (2009) 687–691.
[23] Dongmei Ban, Ningsheng Xu, Shaozhi Deng, Jun Chen, Juncong She, J. Mater. Sci. Technol. 26 (2010) 584–588.
[24] Zu Rong Dai, Zheng Wei Pan, Zhong L. Wang, Adv. Funct. Mater. 13 (2003) 9–24.
[25] I.B. Troitskaia, T.A. Gavrilova, S.A. Gromilov, D.V. Sheglov, V.V. Atuchin, R.S. Vemuri, C.V. Ramana, Mater. Sci. Eng. B. 174 (2010) 159–163.
[26] V. Nirupama, K.R. Gunasekhar, B. Sreedhar, S. Uthanna, Curr. Appl. Phys. 10 (2010) 272–278.
[27] S. Subbarayudu, V. Madhavi, S. Uthanna, Adv. Mater. Lett. 4 (2013) 637–642.
[28] S.H. Mohamed, O. Kappertz, J.M. Ngaruiya, T.P. Leervad Pedersen, R. Drese, M. Wuttig, Thin Solid Films 429 (2003) 135–143.
[29] Se Hee Lee, Maeng Je Seong, C. Edwin Tracy, Angelo Mascarenhas, J. Roland Pitts, Satyen K. Deb, Solid State Ionics 147 (2002) 129–133.
[30] N. Desikan, L. Huang, S.T. Oyama, J. Phys. Chem. 95 (1991) 10050–10056.
[31] Perry A. Spevack, N.S. Mcintyre, J. Phys. Chem. 97 (1993) 11020–11030.
[32] David Yao, Jian Zhen Ou, Kay Latham, Serge Zhuiykov, Anthony Peter O'Mullane, Kourosh Kalantar-zadeh, Cryst. Growth Des 12 (2012) 1865–1870.
[33] Jian Zhen Ou, Jos L Campbell, David Yao, Wojtek Wlodarski, Kourosh Kalantar-Zadeh, J. Phys. Chem. C. 115 (2011) 10757–10763.
[34] O. Goiz, F. Chávez, C. Felipe, N. Morales, R. Pena Sierra, Mater. Sci. Eng. B. 174 (2010) 174–176.
[35] K.P.S.S. Hembram, Rajesh Thomas, G. Mohan Rao, Appl. Surf. Sci. 256 (2009) 419–422.
[36] R. Senthilkumar, T. Mahalingam, G. Ravi, Appl. Surf. Sci. 362 (2016) 102–108.
[37] Chao-Sheng Hsu, Chih-Chieh Chan, Hung-Tai Huang, Chia-Hsiang Peng, Wen-Chia Hsu, Thin Solid Films 516 (2008) 4839–4844.
[38] C.V. Ramana, V.V. Atuchin, V.G. Kesler, V.A. Kochubey, L.D. Pokrovsky, V. Shutthanandan, U. Becker, R.C. Ewing, Appl. Surf. Sci. 15 (2007) 5368–5374.
[39] H.M. Farveez Ahmed, Noor Shahina Begum, Bull. Mater. Sci. 36 (2013) 45–49.
[40] Todd M. McEvoy, Keith J. Stevenson, Langmuir 192 (2003) 4316–4326.
[41] Richard L. Smith, Gregory S. Rohrer, J. Catal. 163 (1996) 12–17.
[42] R. Sivakumar, V. Vijayan, V. Ganesan, M. Jayachandran, C. Sanjeeviraja, Smart Mater. Struct. 14 (2005) 1204–1209.
[43] Hyeyoung Kim, Karuppanan Senthil, Kijung Yong, Chem. Phys 120 (2010) 452–455.
[44] Popatrao N. Bhosale, et al., New J. Chem. 38 (2014) 5964–5974.
[45] Wenzhang Li, Jie Li, Xuan Wang, Jun Ma, Qiyuan Chen, Int. J. Hydrogen Energy 35 (2010) 13137–13145.
[46] W. Li, J. Li, X. Wang, S. Luo, J. Xiao, Q. Chen, Electrochim. Acta 56 (2010) 620–625.
[47] C. Das, I. Paramasivam, N. Liu, P. Schmuki, Electrochim. Acta 56 (2011) 10557–10561.
[48] Todd M. Mcevoy, Keith J. Stevenson, Langmuir 19 (2003) 4316–4326.
[49] K.R Murali, K. Srinivasan, D.C. Trivedi, Mater. Lett. 59 (2005) 15–18.
[50] C. Soci, A. Zhang, B. Xiang, S.A. Aplin Dayeh, J. Park, X.Y. Bao, Y.H. Lo, D. Wang, Nano Lett 7 (2007) 1003–1009.
[51] B. Alotaibi, M. Harati, S. Fan, S. Zhao, H.P.T. Nguyen, M.G. Kibria, Z. Mi, Nanotechnology 24 (2013) 175401–175405.
[52] Toshiaki Mori, Akira Miyamoto, Naoki Takahashi, Masato Fukagaya, Tadashi Hattori, Yuichi Murakami, J. Phys. Chem. 90 (1986) 5197–5201.
[53] P. Ivanov, J. Hubalek, K. Malysz, J. Prasek, X. Vilanova, E. Llobet, X. Correig, Sens. Actuators B 100 (2004) 221–227.
[54] C. Ruan, M. Paulose, O.K. Varghesev, C.A. Grimes, Sol. Energy Mater. Sol. Cells. 90 (2006) 1283–1295.